Applied Catalysis A: General 456 (2013) 144–158

Contents lists available at SciVerse ScienceDirect

Applied Catalysis A: General

journal homepage: www.elsevier.com/locate/apcata

Electrochemical strategy for grown ZnO nanoparticles deposited onto HY zeolite with enhanced photodecolorization of methylene blue: Effect of the formation of Si—O—Zn bonds

N. Sapawe[a], A.A. Jalil[a,*], S. Triwahyono[b], R.N.R.A. Sah[a], N.W.C. Jusoh[a], N.H.H. Hairom[c], J. Efendi[b]

[a] Institute of Hydrogen Economy, Faculty of Chemical Engineering, Universiti Teknologi Malaysia, 81310 UTM Johor Bahru, Johor, Malaysia
[b] Ibnu Sina Institute for Fundamental Science Studies, Faculty of Science, Universiti Teknologi Malaysia, 81310 UTM Johor Bahru, Johor, Malaysia
[c] Department of Water and Environmental Engineering, Faculty of Civil and Environmental Engineering, Universiti Tun Hussein Onn, 86400 Batu Pahat, Johor, Malaysia

ARTICLE INFO

Article history:
Received 13 October 2012
Received in revised form 14 February 2013
Accepted 25 February 2013
Available online 4 March 2013

Keywords:
EGZnO/HY
Electrochemical
Isomorphous substitution
Photodecolorization
Methylene blue

ABSTRACT

Nanoparticles of electrogenerated zinc-supported HY zeolite (EGZnO/HY) catalyst were prepared by a simple electrochemical method. The interaction between zinc species and HY support during the electrolysis was found to affect the EGZnO/HY structure. In addition to the formation of EGZnO nanoparticles (<30 nm in size) that distributed on the surface of HY support, an isomorphous substitution of Al with Zn also occurred in the aluminosilicate framework to result in a Si—O—Zn bonds. The photoactivity of EGZnO/HY was tested on the decolorization of methylene blue (MB). An amount of 0.375 g L^{-1} of 1 wt% EGZnO/HY was found to be the optimum dosage for 10 mg L^{-1} MB, which resulted in 80% of maximum decolorization after 6 h of contact time at pH 3 under fluorescent light (420 nm). Increasing the EGZnO loading led to additional formation of Si—O—Zn bonds and lessened the number of EGZnO nanoparticles, which then reduced the photodecolorization percentage of MB.The photocatalytic reaction was follows the first-order Langmuir–Hinshelwood model, and gives partially mineralization. The photocatalyst was still stable after five cycling runs with no Zn leaching.

1. Introduction

Recently, an environmental problem of water pollution due to rapid industrialization has drawn considerable attention among scientific communities. Approximately 22% of the total volume of industrial wastewater was generated, which comes from the textile industry whereas over 100,000 dyes were available with more than 7×10^5 tons of dyestuff produced annually [1,2]. However, most of the unused dye produces undesirable effluents, which are discharged into the environment with or without further treatment. These effluents enter natural water bodies and can cause severe problems if not treated properly because the dyes are toxic, mutagenic, and carcinogenic to human life [3] as well as inhibit photosynthesis of aquatic life even in small quantities such as 1 ppm [4]. To overcome this problem, several methods for the removal of dyes have been reported, including chemical and biological oxidation [5], adsorption [6], coagulation and flocculation [7], electrochemical oxidation [8], ion exchange [9] and membrane separation [10]. However, these methods have their own limitations of being time consuming, expensive, and commercially unattractive as well as resulting in the generation of secondary wastes.

Advanced oxidation processes (AOPs) using semiconductor metal oxides, such as TiO_2, WO_3, Fe_2O_3, ZnO, CuO, ZrO_2, CdS, In_2O_3, and SnO_2, as photocatalysts have become important because the AOPs can convert a wide range of harmful dyes into non-toxic products, CO_2, and water at ambient temperature [11–13]. In addition, the use of mesoporous materials, such as zeolite, as a support for the metal oxides has recently become the focus of intensive research because the catalyst support influences the catalytic performance through structural features and the interaction between the materials leads to enhancement of the contact between the surface and the irradiation [14] as well as reduction in the amount of metal oxides required [13]. A review of recent studies has revealed that some of the important metal oxide-supported zeolites include TiO_2-HZSM-5, Co-ZSM-5, CuO-X zeolite, and Fe-exchange zeolite [15–18]. The most popular metal oxides used were TiO_2 and ZnO, but in particular, ZnO has attracted much attention with respect to its ability to degrade various pollutants due to its high photosensitivity and

* Corresponding author. Tel.: +60 7 5535581; fax: +60 7 5536165.
E-mail address: aishah@cheme.utm.my (A.A. Jalil).

0926-860X/$ – see front matter © 2013 Elsevier B.V. All rights reserved.
http://dx.doi.org/10.1016/j.apcata.2013.02.025

stability as well as suitable alternative to TiO_2 since it has similar band gap energy, which is equal to 3.20 eV [19,20]. To the best of our knowledge, reports on ZnO-supported zeolite as photocatalysts are still scarce.

The nanosized ZnO has evoked a great deal of interest in recent years, especially in the area of photocatalytic studies for enhancing its performance such as an increase in surface area and changes in surface properties as well as in quantum effect of photocatalyst materials [20–22]. Upon light irradiation, this nanosized ZnO generated a highly active radical species, thus it can easily oxidize an organic waste such as dyes into less harmful residues [22,23]. Various routes to synthesize nanosized zinc particles such as sol–gel, hydrothermal, alkali precipitation, thermal decomposition, organo-zinc hydrolysis, spray pyrolysis, microwave irradiation, and sonochemical synthesis [20,24–26] have been reported, but there are still limitations to study the preparation of nanosized zinc particle using electrochemical technique.

We have reported a new method for preparing very fine particles of electrogenerated zinc metal (EGZn) with high reactivity using a simple electrochemical method and its successful use in the synthesis of anti-inflammatory agents [27]. It was also found that the zinc oxide nanoparticles (EGZnO) led to the generation of protonic acid sites when supported on HZSM-5, which enhanced the *n*-alkane isomerization [28]. By the corresponding method, an α-Fe_2O_3 and $EGZrO_2$ supported HY catalyst was also successfully achieved, which possesses high photoactivity in the decolorization of methyl orange and methylene blue, respectively [29,30].

Additionally, exploring a new application dealing with the use of the nanoparticles EGZnO would be of interest, particularly in the area of photocatalytic reaction. Therefore, in the present study, we report for the first time, the preparation of EGZnO supported on HY zeolite (EGZnO/HY) and its photoactivity toward a decolorization of methylene blue (MB). The prepared catalyst was characterized by X-ray diffraction (XRD), thermogravimetric simultaneous differential thermal analysis (TG-SDTA), field emission scanning electron microscopy coupled with energy dispersive X-ray (FE-SEM/EDX), transmission electron microscopy (TEM), Fourier transform infrared (FTIR), ultraviolet–vis diffuse reflectance spectroscopy (UV–vis DRS), photoluminescence (PL), Brunnauer–Emmett–Teller (BET) surface area analysis, ^{29}Si and ^{27}Al magic angle spinning nuclear magnetic resonance (MAS NMR), X-ray photoelectron spectroscopy (XPS), and inductively coupled plasma mass spectrometry (ICP-MS). A new structural model for EGZnO/HY was proposed on the basis of characterization and photodecolorization results. The decolorization of MB was optimized under various parameters such as the effect of pH, EGZn loading, catalyst dosage, and initial MB concentration. The kinetics behavior of the catalyst was also studied to determine the surface interaction of the catalyst with MB.

2. Experimental

2.1. Materials

The HY zeolite had a Si/Al ratio of 80 and was purchased from Zeolyst International. *N*,*N*-dimethylformamide (DMF) was purchased from Merck and naphthalene was obtained from Fluka. Sodium hydroxide (NaOH), hydrochloric acid (HCl), hydrogen peroxide (H_2O_2), and methylene blue (C.I. 52015 for microscopy) were obtained from QReC™. Ammonium oxalate was purchased from Riedel–De Haen AG Seelze–Hannover while isopropanol was purchased from Systerm®. The platinum (Pt) and zinc (Zn) plate cells were obtained from Nilaco Metal, Japan. All reagents were of analytical grade and were used as received. Deionized water was used for the preparation of the pH solution and adjustments to the pH were performed using a 0.1 M HCl and NaOH solution.

2.2. Catalyst preparation

EGZnO was prepared following a previously reported protocol [27,31]. A DMF solution (10 mL) containing 0.1 M tetraethylammonium perchlorate was electrolyzed in the presence of a naphthalene mediator (6 mmol) in a normal one-compartment cell fitted with a Pt plate cathode (2 cm × 2 cm) and Zn plate anode (2 cm × 2 cm) at a constant current density of 120 mA/cm^2 under a nitrogen atmosphere at 273 K. After electrolysis, the mixture was impregnated, oven dried overnight at 378 K, and calcined at 823 K for 3 h to yield a white powder (EGZnO) for characterization and photocatalytic testing.

The EGZnO/HY catalyst was prepared using the same procedure except for the addition of the HY zeolite (1.5 g) prior to electrolysis, and a white powder was obtained as the final product. The required weight percent of the EGZnO supported on HY and the time required for complete electrolysis was calculated based on Faraday's law of electrolysis,

$$t = \left(\frac{F}{I}\right)(z \times n) \quad (1)$$

where t = total time for the constant current applied (s); F = 96,486 C mol^{-1}, which is the Faraday constant; I = the electric current applied; z = the valency number of ions of substances (electrons transferred per ion); and n = the number of moles of Zn (no of moles, liberated n = m/M).

2.3. Characterization

The crystalline structures of the catalysts were studied by XRD recorded on a D8 ADVANCE Bruker X-ray diffractometer using Cu K_α radiation at a 2θ angle ranging from 3° to 90°. The particle sizes of the catalysts were calculated using the Debye–Scherrer equation,

$$D = \frac{k\lambda}{\beta \cos\theta} \quad (2)$$

where k = 0.94 is a coefficient, λ = 1.5406 Å is the X-ray wavelength, β is the full width half maximum (FWHM) of the sample and θ is the diffracting angle. The phases were identified with the aid of the Joint Committee on Powder Diffraction Standards (JCPDS) files.

The thermal stability behavior of establish catalysts was examined by thermogravimetric simultaneous differential thermal analysis (TG-SDTA) (TGA/SDTA851 Instrument). The measurement was carried out from 278 to 1173 K with heating rate of 278 K min^{-1} under nitrogen flow at rate of 40 mL min^{-1}. The topological properties as well as semi-quantitative determination of percentage metal loaded were observed by field emission scanning electron microscopy coupled with energy dispersive X-ray spectrometer (FE-SEM/EDX) (JSM-6701F). The morphological properties of nanosized EGZnO and the EGZnO/HY catalyst as well as the distribution of EGZnO deposited on the HY surface were examined by TEM (JEOL JEM-2100F). FTIR (Perkin Elmer Spectrum GX FTIR Spectrometer) was performed using the KBr method with a scan range of 400–4000 cm^{-1}. The optical absorption properties of the catalyst were obtained using a UV–vis DRS (Perkin Elmer Spectrophotometer) in the range of 200–800 nm at room temperature. The photoluminescence (PL) (JASCO Spectrofluorometer) (FP-8500) with 150 W Xe lamp as excitation source were employed to study the electronic structure, optical and photochemical properties of semiconductor materials, by which information such as surface oxygen vacancies and defects, as well as the efficiency of charge carrier trapping, immigration and transfer can be obtained. The band gap of EGZnO was determined from plots of the Kubelka–Munk (K–M) function [$f_{K\text{-}M} = (h\nu/\lambda)^{1/2}$] as a function of the energy of the excitation light [$h\nu$].

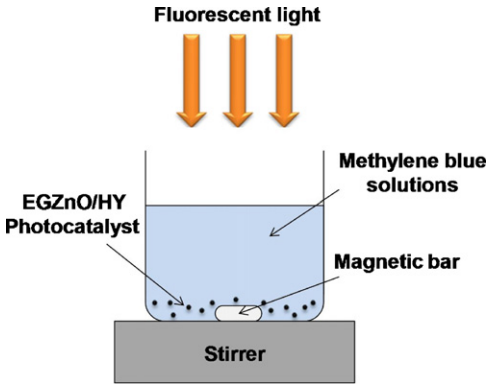

Fig. 1. Schematic diagram of the photocatalytic reaction.

The textural properties (i.e., specific surface area, pore volume, and pore diameter) were determined from nitrogen adsorption–desorption isotherms at liquid nitrogen temperature using a Micromeritics ASAP 2010 instrument. The surface area was calculated with the BET method, and pore distributions were determined by the Barrett–Joyner–Halender (BJH) method. Prior to measurement, all the samples were degassed at 383 K to 0.1 Pa. ^{29}Si and ^{27}Al MAS NMR spectra were recorded on a Bruker Solid NMR (JEOL 400 MHz) spectrometer using tetramethylsilane (TMS) as an external reference at room temperature. The chemical oxidation state of the EGZnO/HY catalyst was determined using XPS conducted on a Kratos Ultra spectrometer equipped with a Mg K_α radiation source (10 mA, 15 kV) in the range of 0–800 eV. The powdered sample was pressed into a small Inox cylinder and analyzed inside an analysis chamber at 1×10^{-10} Pa during data acquisition. To correct the energy shift due to surface charging of the samples, the binding energy of the C_{1s} peak at 284.5 ± 0.1 eV was taken as the internal standard.

2.4. Photocatalytic testing

The photocatalytic activity of the prepared EGZnO/HY catalyst was tested for the decolorization of MB, and a simple schematic diagram used for the testing is shown in Fig. 1. A 0.075 g sample of the catalyst was dispersed in 200 mL of 10 mg L^{-1} MB aqueous solution. The adsorption–desorption equilibrium was achieved under dark conditions after 2 h, and the mixture was irradiated at room temperature for 6 h with constant stirring using a fluorescent lamp (Philips TLD 36 W/865; 15,000 h; 6500 K; 420 nm emission). At specific time intervals, 2.5 mL of the sample solution was withdrawn and centrifuged prior measurements of the MB concentration by a UV–vis spectrophotometer (Thermo Scientific Genesys 10 uv Scanning) using the characteristic adsorption band at 664 nm. The decolorization percentage was calculated as follows,

$$\text{decolorization}\,(\%) = \frac{(C_0 - C_t)}{C_0} \times 100 \quad (3)$$

where C_0 represents the initial concentration and C_t denotes a variable concentration.

The effect of different scavengers on photocatalytic performance was also carried out using ammonium oxalate (0.15 g), isopropanol (10%, v/v), and hydrogen peroxide (10%, v/v).

2.5. Analyses

The elemental analyses of Zn in a solution during an experiment were determined by ICP-MS using ELAN 6100 PerkinElmer ICPMS. The biochemical oxygen demand (BOD) of the solution were measured using YSI model 33, whereas the BOD bottles were incubated at 293 K for five days and the difference in dissolved oxygen was used to calculate BOD_5. The HACH DR4000 spectrometer was used for chemical oxygen demand (COD) measurement. In addition, the total organic carbon (TOC) removal was determined using a TOC Shimadzu Vcph spectrophotometer for each run before and after a 6 h reaction time for the evaluation of the mineralization of MB dye. TOC was calculated as the difference between the total carbon (TC) and inorganic (IC) in the liquid sample.

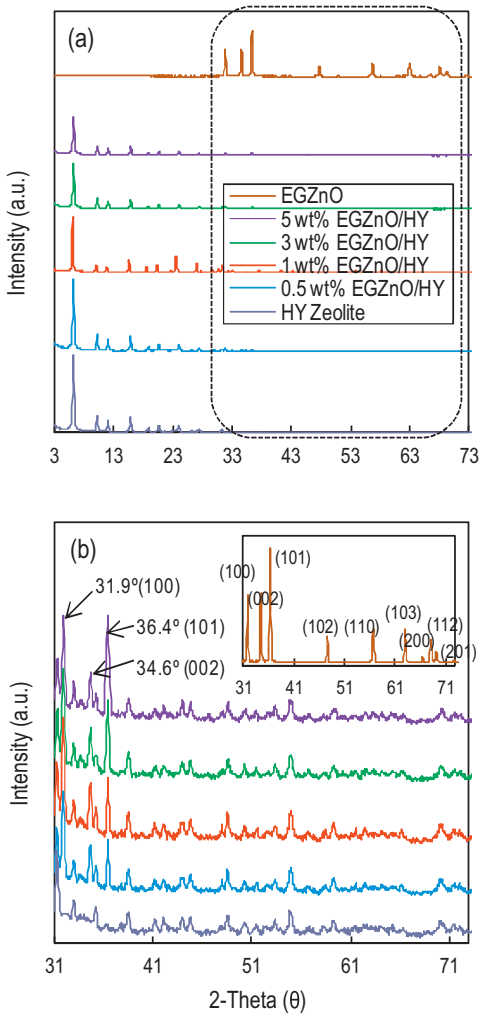

Fig. 2. XRD patterns of catalysts for (a) full range 3–73° and (b) range 31–71°.

3. Results and discussion

3.1. Characterization

3.1.1. Crystallinity, phase and structural studies

The XRD pattern of the prepared EGZnO/HY catalysts were compared with EGZnO and bare HY, and the results are shown in Fig. 2. The peak intensity of HY decreased as the EGZnO loading increased because the presence of foreign substances affected the morphology of the supported HY fingerprint (Fig. 2a). A series of characteristic peaks were observed for EGZnO at 31.9° (1 0 0), 34.6° (002), 36.4° (1 0 1), 47.7° (1 0 2), 56.7° (1 1 0), 63.0° (1 0 3), 66.5° (2 0 0), 68.1° (1 1 2), and 69.2° (2 0 1), which were in accordance with those of the hexagonal wurtzite structure of ZnO (International Center for Diffraction Data, JCPDS 36-1541) [20]. However, no other diffraction peaks were detected, which indicated the purity of

Table 1
The crystallite size and d_{101} value of the catalysts.

Catalysts	Crystallite size (nm)	d_{101} value (Å)
EGZnO	30.5	2.47
HY Zeolite	33.2	–
0.5 wt% EGZnO/HY	40.8	2.47
1 wt% EGZnO/HY	40.8	2.47
3 wt% EGZnO/HY	27.2	2.47
5 wt% EGZnO/HY	24.5	2.47

the prepared EGZnO. The enlargement of selected area XRD pattern in Fig. 2a from 31° to 71° for each weight percent loading is shown in Fig. 2b. The three peaks located at 31.9° (1 0 0), 34.6° (0 0 2), and 36.4° (1 0 1) correspond to ZnO, thereby verifying the presence of EGZnO metal on the framework of HY.

The average crystallite size of the catalysts was estimated by the Debye–Scherrer equation on the basis of major peak of EGZnO (101) at $2\theta = 36.4$ to have d_{101} values of approximately 2.47 Å and these values are listed in Table 1. The crystallite size decreased as with EGZnO, and the values ranged from 40.8 to 24.5 nm due to the interaction and agglomeration between the zinc species and HY [32].

3.1.2. Thermal stability of photocatalysts

The thermogravimetric analysis curves of HY zeolite and EGZnO/HY are presented in Fig. 3. The HY showed only small endothermic weight loss (4%) in the range of 293–403 K, attributed to water removal (Fig. 3a). In case of EGZnO/HY (Fig. 3b), the behavior is completely different; two types of endothermic weight losses were detected, from room temperature to 513 K (20%) and at 1123–1173 K (4%). The former interpreted the elimination of surface water and a few volatile compounds, which were used during the preparation of EGZnO/HY. The latter may indicate the formation of Zn intermediates as reported in [33].

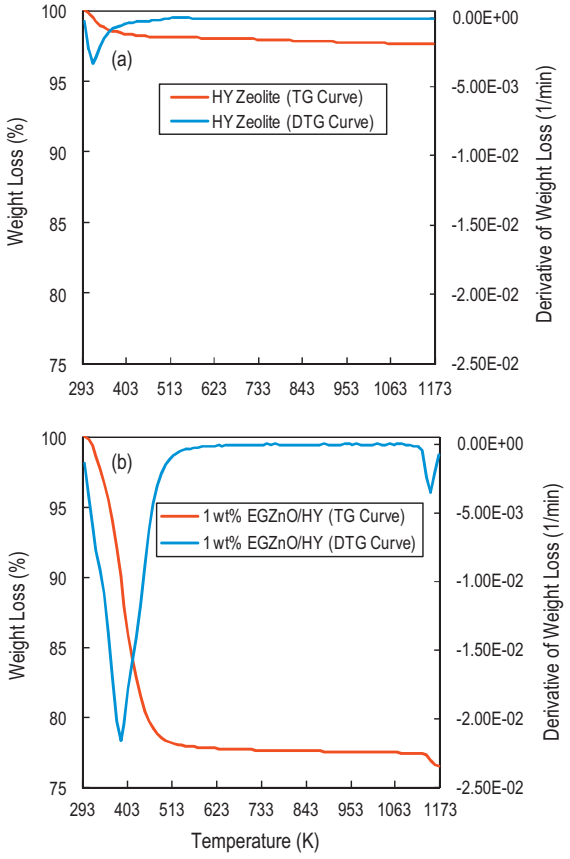

Fig. 3. TG/DTG thermograms of (a) HY zeolite and (b) 1 wt% EGZnO/HY.

3.1.3. Topological properties

The topological properties of the EGZnO and EGZnO/HY catalysts were studied by FE-SEM and the results are shown in Fig. 4. The influence of the addition of zinc on the HY zeolite structure can also be confirmed from SEM images. The micrographs showed the presence of small crystallites uniformly distributed along some intergrowth. It can be seen that nanosized EGZnO particle less than 30 nm in size with uniform shape was successfully synthesized and they exist in single homogeneous phase with narrow size distribution and agglomerate with each other (Fig. 4a and b). It is demonstrated that the morphology and particle size of EGZnO/HY catalysts did not change with respect to those of HY zeolite, indicating that no crystalline transformations occurred during the addition of zinc onto HY zeolite. Zinc oxide were finely dispersed as their presence did not result in significant contrast at magnifications up to 30 000×. A smooth surface was observed in 1 wt% EGZnO/HY (Fig. 4d), and further increase in percentage loading up to 3 wt% and 5 wt% EGZnO/HY (Fig. 4c, e, and f) demonstrated a rough surface with extent to some agglomeration between particles. Such roughness provided a limited contact angle area to light penetration, thereby reducing the utilization rate of photodecolorization of MB [34].

The EDX analysis was employed to determine the composition of the EGZnO (Table 2). The peaks of Zn and O correspond to ZnO and Al and that of Si to HY, whereas Pt and C originated from the coated material as well as the platform of the holder sample. No other element was detected, indicating that EGZnO/HY is free from other impurities. From the semi-quantitative analysis, we can estimate the amount of EGZnO loading onto the HY.

3.1.4. Morphological properties

The morphological properties of the EGZnO and EGZnO/HY catalysts were examined by HR-TEM, and the images are presented in Fig. 5. Fig. 5a and b illustrates that the EGZnO was successfully prepared with well-defined boundaries and no connecting necks, which indicated the absence of sintering effect between the particles. The average particle size for EGZnO varied in a narrow range from 10 to 30 nm, which is parallel to FE-SEM analysis results. The theoretical value of the particle size (D) was found to be 29.7 nm, which was estimated from the following equation,

$$D = \frac{6}{\rho S} \tag{4}$$

where ρ is the theoretical density of the EGZnO powder and S is the surface area determined by N_2 adsorption–desorption isotherms assuming that the particles are spherical in shape [35].

However, the micrographs show particles with elliptical and irregular shapes, which may be due to overlapping of particles [36]. The inset figures are the fast Fourier transform patterns (FFT) and indicate that the materials either have a crystalline (Fig. 5b and g) or an amorphous (Fig. 5d) phase. Magnification of the selected area in the FFT patterns showed the atomic arrangement in the crystal and allowed the estimation of the interplanar distance (Fig. 5c and h). The value of the interplanar distance (d-spacing) of the lattice fringes estimated from this image was consistent with the value of lattice spacing of EGZnO obtained from the XRD analysis at d_{101} (2.47 Å) and d_{002} (2.59 Å). This agreement confirms that the EGZnO nanoparticles were deposited and well dispersed on the HY support as seen in Fig. 5e–g.

3.1.5. Vibrational spectroscopy

FTIR spectroscopy is a very useful technique for obtaining vibrational information about the species in materials. Therefore, the

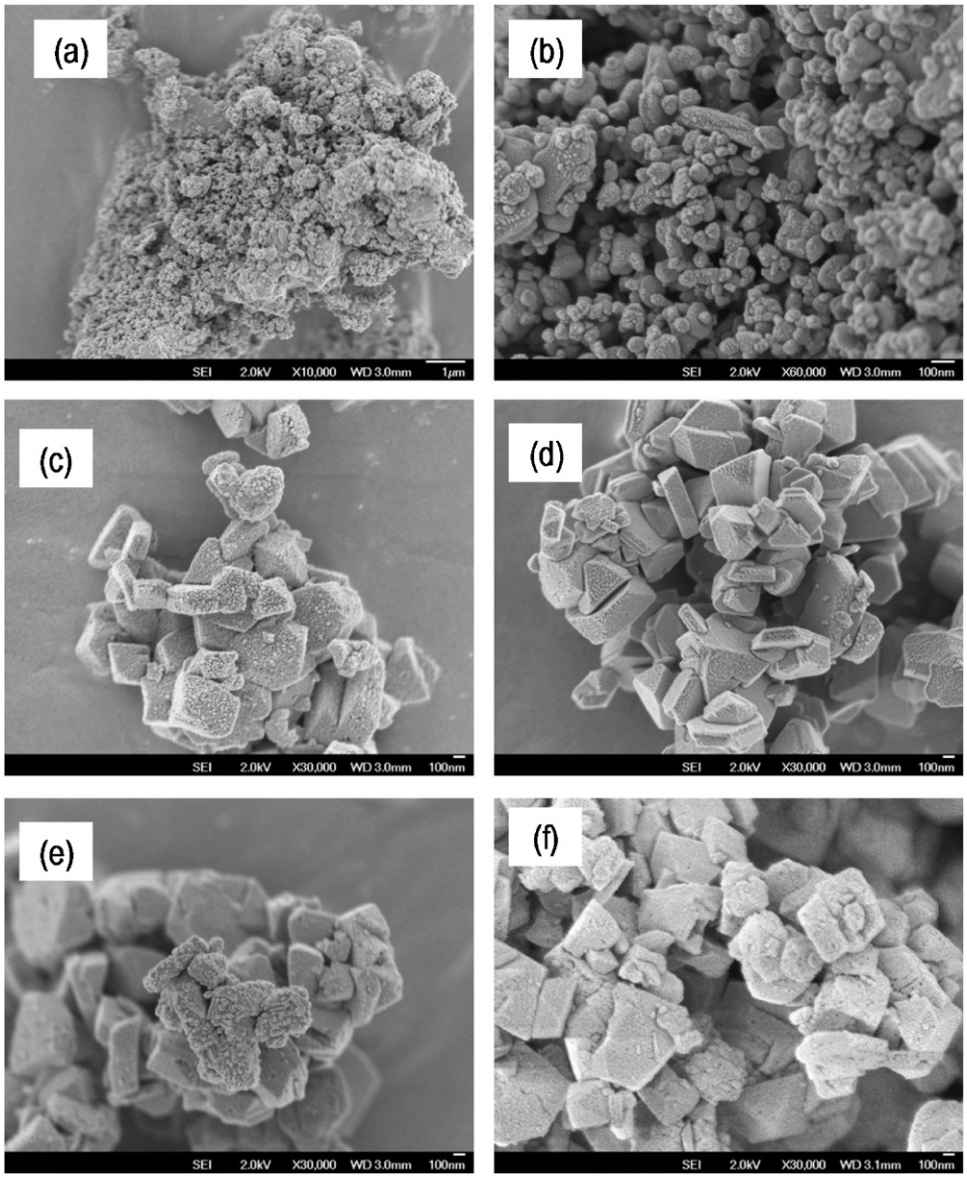

Fig. 4. FE-SEM images of (a, b) EGZnO in low and high magnification (c) 0.5 wt% EGZnO/HY (d) 1 wt% EGZnO/HY (e) 3 wt% EGZnO/HY (f) 5 wt% EGZnO/HY.

prepared catalysts were subjected to FTIR analysis, and the results are shown in Fig. 6. The EGZnO/HY catalyst showed broad band at 3445 cm^{-1} due to the H_2O molecules adsorbed on catalyst surface and 1634 cm^{-1}, which was attributed to the vibrational distortion of O—H groups on the catalyst surface (Fig. 6a). The weak bands between 800 and 400 cm^{-1}, which correspond to the Si—O—Si flexural vibration, decreased in intensity as with the EGZnO loading because of the superposition of Zn—O and Si—O bonds (Fig. 6a) [37]. A significant decrease in the intensity of the peak at 1079 cm^{-1} was observed after EGZnO loading, which suggested a possible interrelationship between EGZnO and the Si—O—Si group (Fig. 6a) [37]. This result suggests that Zn may be inserted into the zeolite framework during electrolysis [38]. However, no obvious band was observed, which corresponds to the vibration of the Si—O—Zn bond. It may be because of overlapping with zeolite characteristic stretching frequencies in the region [39]. For further investigation, the samples were evacuated at 673 K for 1 h prior to IR measurement to remove the physisorbed water, and the results are shown

Table 2
Elemental compositions of catalysts determined by EDX analysis.

Catalysts	Elemental compositions (%)						Total (%)
	C	O	Zn	Si	Al	Pt	
EGZnO	1.22	3.02	88.92	–	–	6.84	100
HY zeolite	8.02	27.21	–	51.17	2.93	10.67	100
0.5 wt% EGZnO/HY	7.12	30.25	0.66	47.24	1.75	12.98	100
1 wt% EGZnO/HY	28.93	26.75	1.95	20.42	3.21	18.74	100
3 wt% EGZnO/HY	30.13	26.87	5.49	22.02	0.26	15.23	100
5 wt% EGZnO/HY	15.67	33.08	7.12	30.02	0.15	13.96	100

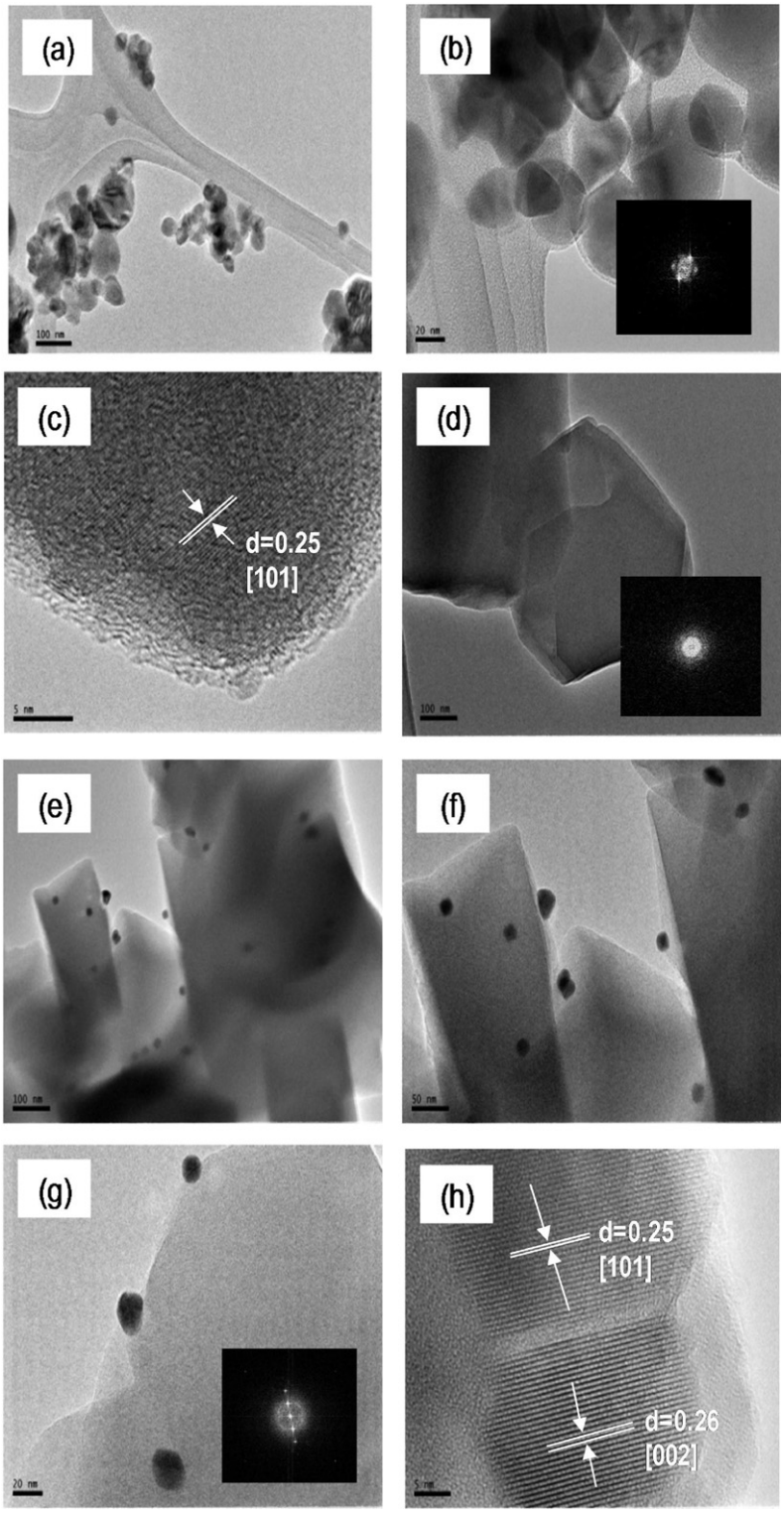

Fig. 5. HR-TEM micrographs of catalysts in low and high magnification for (a–c) EGZnO (d) HY zeolite (e–h) EGZnO/HY and the insert of Fig. 4 (b, d, and g) are its corresponding FFT.

in Fig. 6b. The sharp peak at 3745 cm^{-1} was shifted to a lower wave number (3740 cm^{-1}) and the intensity increased with EGZnO loading, which could be attributed to a weak interaction between the isolated silanol groups located at the surface and the neighboring metal species (Zn) [40]. According to Krijnen, the shift in this peak to 3740 cm^{-1} may also suggest that dealumination has occurred in the zeolite [41]. The peak at 3700 cm^{-1} decreased in intensity with metal loading, which may correspond to the interaction of Zn species with weak hydrogen bridges in defect sites of hydroxyl groups. A new peak appeared at 3685 cm^{-1}, which increased in intensity with EGZnO loading, indicating the increase of the hydroxyl groups of the extra framework aluminum species due to the ion exchange between Zn and Al ions in the framework [41].

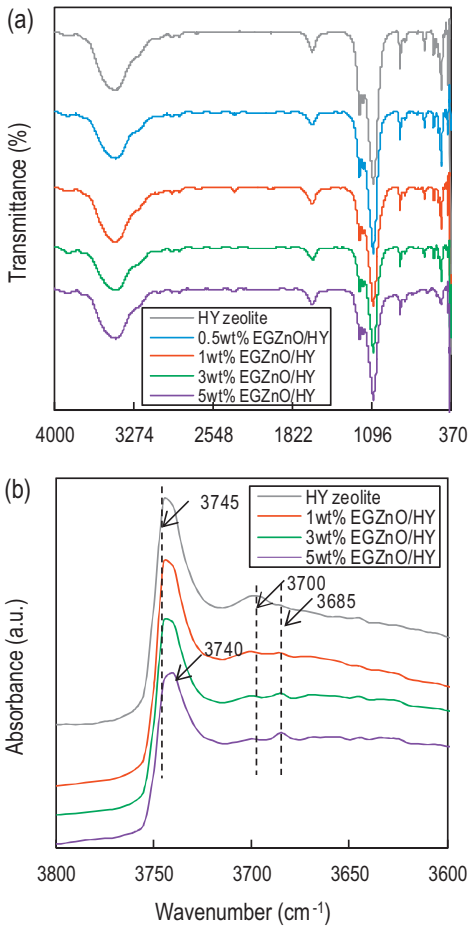

Fig. 6. FTIR spectra of catalysts at region (a) 4000–370 and (b) 3800–3600 cm^{-1} (evacuated system).

3.1.6. Nuclear magnetic resonance

To elucidate the structure of the prepared catalyst, ^{29}Si and ^{27}Al MAS NMR spectra were obtained for the 5 wt% EGZnO/HY with respect to bare HY. ^{29}Si MAS NMR chemical shifts were used to define the Si environments and provide information regarding the coordination of Si with other Si or Al atoms. As illustrated in Fig. 7a, the intensity of the sharp peak observed for bare HY at −107 ppm was reduced by approximately 30% upon the introduction of EGZnO, which could indicate dealumination effect or isomorphous substitution with zinc [42]. ^{27}Al MAS NMR was employed to distinguish the Al in framework sites (tetrahedral) from extra framework sites (octahedral). In Fig. 7b, the peak corresponding to the tetrahedral Al framework in HY was eliminated when EGZnO was added. However, no other peaks were detected signifying neither the presence of octahedral extra framework aluminum nor the reinsertion of the eliminated aluminum into the Si framework [43,44]. As reported by Klinowski, the eliminated aluminum may be present as *invisible* aluminum such as $Al(OH)_3$, $Al(OH)^{2+}$, $Al(OH)^{+}_2$, and Al_2O_3 or as certain polymeric aluminous species [42].

To clarify the isomorphous substitution between Zn and Al, the amount of unbounded Zn and Al in the HY framework was studied using 5 wt% EGZnO/HY catalyst. The corresponding catalyst was stirred in DMF solution for approximately 30 min and then filtered before subjecting to ICP-MS analysis. It was found that approximately 1.96×10^{20} Zn atoms were detected in the filtrate solution, referring to the unbounded EGZnO (27%). Therefore, 73% of total Zn ions in 5 wt% EGZnO/HY catalyst were exchanged with the Al in HY framework. However, the number of Al atoms detected from the same solution was 2.18×10^{21}, which was more than estimated number of Al that were exchanged with the Zn in the aluminosilicate framework. The superfluous amount of Al (1.65×10^{21}) is most probably due to dealumination, whereas the remaining undetected Al (~30%) might correspond to polymeric aluminous compounds that could not pass through the filter as reported in NMR studies. All the calculations were based on the ratio of element in the HY $(Al_7Si_{17}O_{48})\cdot 32(H_2O)$.

3.1.7. Chemical oxidation state determination

The dealumination of zeolite after the addition of zinc was confirmed by the FTIR and NMR data. XPS analyses were performed to determine the chemical states of the surface Zn in the catalyst. Fig. 8 shows the XPS spectra of $Zn_{2p3/2}$ and O_{1s} for the 5 wt% EGZnO/HY catalyst. The deconvolution of $Zn_{2p3/2}$ shows the existence of two peaks. The peak at 1023.0 eV was similar to the uniform oxidation state of Zn^{2+} [45,46]. The observed value was slightly higher than that reported for pure zinc oxide probably because of the interaction between EGZnO and HY [47]. The low intensity peak at lower binding energy (1021.1 eV) signifying the formation of Zn species incorporated with zeolite framework [45].

In addition, the spectra of O_{1s} were obtained to differentiate the bonded oxygen atoms in silica environments. The photoelectron spectra of O_{1s} shown in Fig. 8 display two oxygen species present in the nearby region that correspond to Si—O—Zn and Si—O—Si with binding energies of 530.5 and 532.8 eV, respectively [48,49]. The peak at 530.5 eV can be indexed to the O^{2-} ions in ZnO lattice or matrix, whereas the peak at 532.8 eV is due to the specific chemisorbed adsorbed oxygen caused by the surface adsorbed hydroxyl, which corresponds to O—Si bonds in the samples [49]. No obvious peaks for other elements or impurities were observed.

3.1.8. Study of optical properties

Fig. 9a shows the UV–vis reflectance spectra of the prepared catalysts with different zinc loading. From the figure, the EGZnO shows a characteristic peak at a wavelength of 386 nm. The decreased in the EGZnO loading from 5 to 0.5 wt% onto HY resulted in increase of peak intensity, and has a spectrum similar to bare HY. This is most probably because of the low metal loading and highly dominant fingerprint of HY frequencies [30,38]. The band gap energy of EGZnO was determined using the Kubelka–Munk (K–M) spectrum by plotting $f_{K-M} = (h\nu/\lambda)^2$ as a function of $h\nu$ (Fig. 9b) [50] and compared to the band gap calculated from $E_b = 1240/\lambda$ [51]. Both the EGZnO band gap values were similar, which were approximately close to 3.20 eV and agreed with those reported in [52]. Generally, the photocatalyst can absorb photon energy that equal or greater than band gap energy and generates photoexcited electron–hole pairs in bulk [53].

3.1.9. Photoluminescence study

Fig. 10 shows the photoluminescence (PL) spectra of bare EGZnO and EGZnO/HY catalysts with excitation wavelength of 325 nm. EGZnO samples exhibit an intense and sharp peak at 386 nm in the UV region, and a broad band at 514 nm in the visible region. The UV emission (near band edge emission) was generated by the free-excitation recombination, while the green emission (deep level emission) was appeared because of the impurities and structural defects in the deposited structures. The UV emission signifies the recombination of a photogenerated hole with an electron occupying the oxygen vacancies, while the green emission signifies the recombination of electrons in single occupied oxygen vacancies in ZnO [21]. Generally, highly crystalline ZnO shows a dominated UV emission with a weak green emission. It is observed that the PL intensity of EGZnO/HY was decreased by the addition of zinc oxide, but 3 wt% EGZnO/HY showed slightly higher PL intensity compared to 1 wt% and 5 wt% EGZnO/HY. This is may be due to the addition

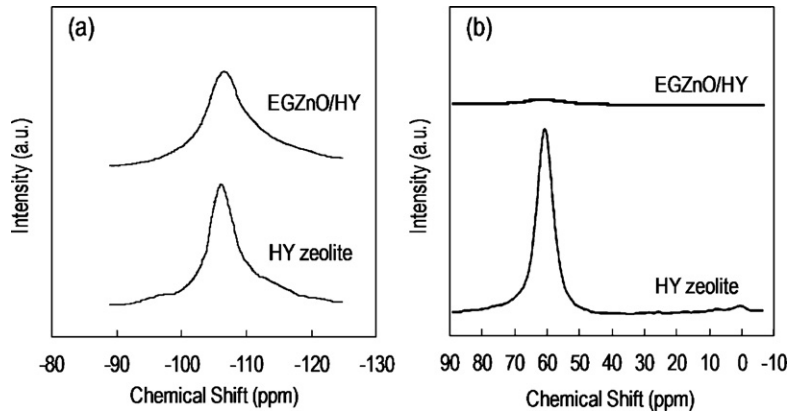

Fig. 7. MAS NMR spectra of (a) ^{29}Si (b) ^{27}Al of bare HY and 5 wt% EGZnO/HY catalyst.

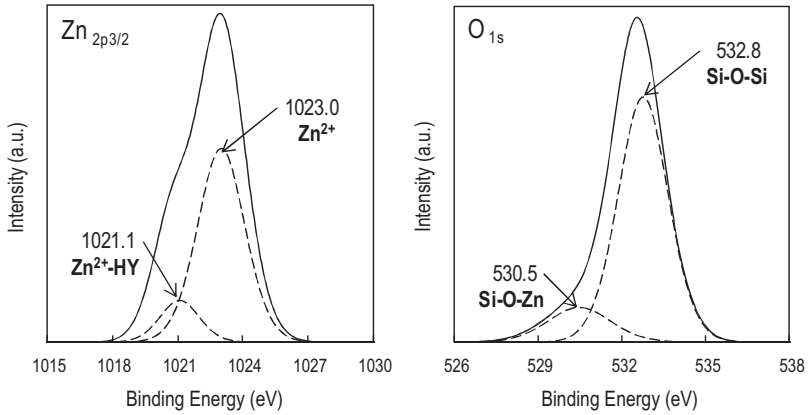

Fig. 8. XPS spectra of $Zn_{2p3/2}$ and O_{1s} for 5 wt% EGZnO/HY catalyst.

of certain amount of Zn could affects the intensity and response range of PL signals which resulted in increase in the content of surface oxygen vacancies and defects [21]. In fact, the lower the PL intensity, the lower the recombination rate of photoinduced electron–hole pairs, which resulted in higher photocatalytic activity of the catalyst [54,55]. Moreover, the peak positions of PL spectra for a different weight percent of the EGZnO/HY catalysts apparently shifted to longer wavelengths, implying the decrease in band gap energy of EGZnO. In contrast, 1 wt% EGZnO/HY catalyst shows a different pattern of PL emissions compared to others, suggesting the existence of different energy levels in the conduction band (CB) to which the electrons in the valence band (VB) can be promoted on the condition of similar excitation energy, and the excited electrons with different energy in the CB can come back to VB via different courses [21]. Thus, 1 wt% EGZnO/HY tends to shifted to the deep level emission in order to exhibit good optical properties, resulting the most effective photocatalyst in this study.

3.1.10. *Proposed structure of EGZnO/HY*

Based on characterization studies, probable reaction pathways to prepare EGZnO/HY are shown in Fig. 11. The electrolysis of DMF solution with a Pt cathode and a Zn anode results in anodic dissolution of Zn metal to give Zn ions. On the other hand, at the cathode, a one-electron reduction of naphthalene ([Naph]) molecule occurs

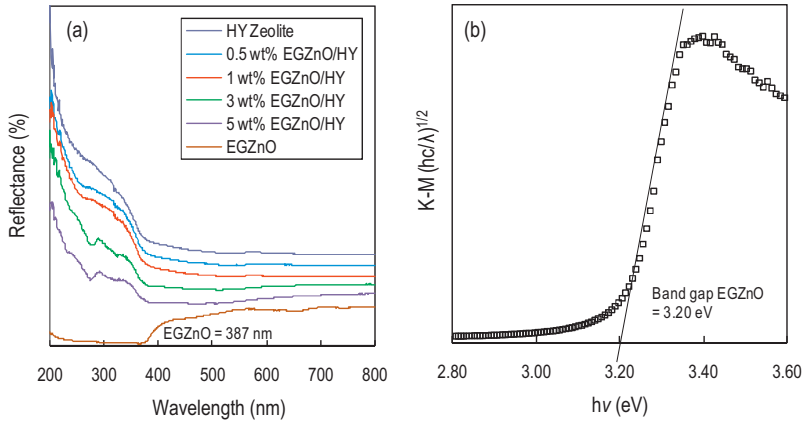

Fig. 9. (a) UV–vis reflectance spectra of catalysts and (b) the $(f_{K\text{-}M})$ vs. $(h\nu)$ spectra of EGZnO.

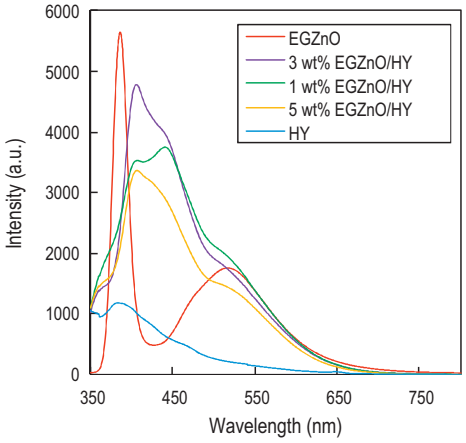

Fig. 10. PL spectra of the catalysts with the excitation wavelength of 325 nm.

to give a radical anion of naphthalene, which was shown by the appearance of a dark green color on the surface of the cathode [27]. The reduction of Zn ion with naphthalene radical anion gave zerovalent highly reactive EGZn, which was oxidized to EGZnO when underwent calcination after the electrolysis. In parallel, a part of the Zn^{2+} ions takes participates in the isomorphous substitution to form EGZnO/HY catalyst.

The FTIR results obtained were in agreement with the data reported by Krijnen, in which the shifted peak from 3745 to 3740 cm^{-1} signifies dealumination in the zeolite framework and the appearance of a new peak at 3685 cm^{-1} indicates the presence of hydroxyl groups of extra-framework aluminum species [41]. In addition, the XPS spectra of $Zn_{2p3/2}$ and O_{1s} established the chemical oxidation state of the Zn^{2+} ions and the presence of Si—O—Zn group, respectively. Therefore, it was proposed that the Al was extracted from the HY framework creating vacant sites, which are then filled by Zn^{2+} during electrolysis (Fig. 11). The dealumination designated by ^{29}Si and ^{27}Al MAS NMR spectra and the total number of unbounded Zn and Al atoms in the HY framework

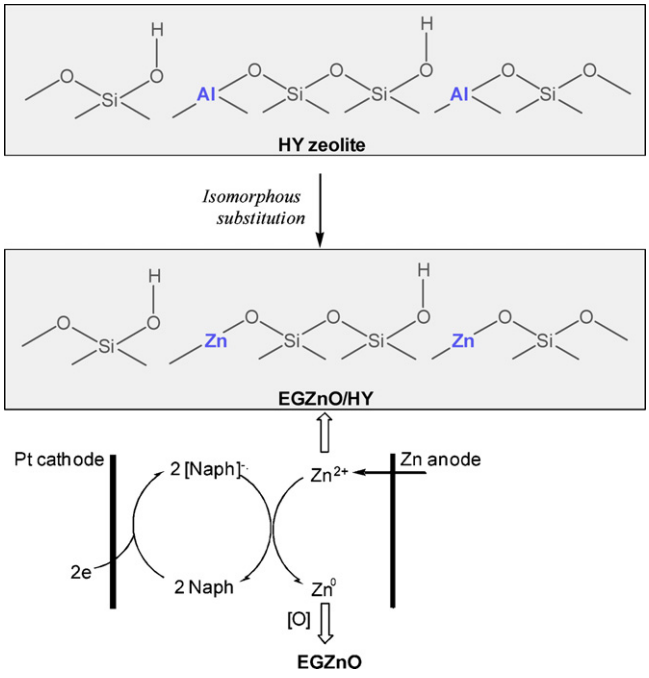

Fig. 11. Proposed mechanism for isomorphous substitution of Al with Zn in the HY zeolite structure.

obtained by ICP-MS results also support the proposed structure. This study has shown that the dealumination could be easily performed by the electrolysis system without using strong acids, reactive compounds, and/or hydrothermal treatment [41]. However, the proposed model of EGZnO/HY depends on the amount of EGZnO loading. Based on FTIR results, it was predicted that higher loading of EGZnO gives higher probability of Si—O—Zn bond formation. This is verified by the increase in intensity of the peak at 3685 cm^{-1}, which is assigned to hydroxyl group of extra framework aluminum species, indicating that more Al ions were dealuminated from the framework, thereby resulting in more Zn ions that will be replaced by the framework.

3.2. Photocatalytic testing for the decolorization of MB

3.2.1. Performance of the EGZnO/HY as a photocatalyst

The performance of prepared EGZnO/HY catalyst was examined for the decolorization of MB, and the results are shown in Fig. 12a. A controlled experiment was conducted under four different conditions including photolysis and reaction in the presence of the bare HY, EGZnO, and EGZnO/HY catalysts. Each experiment was performed under both dark and visible light conditions. The experiments under dark conditions removed less than 26% of the MB after 6 h of contact time, which indicated the importance of visible light in this study, as revealed by the optical properties study. Under photolysis, 0.96% of the MB was decolorized; this may be because of the degradation of the substance after long exposure to fluorescent light. Only 13.2% and 23.5% of the MB was removed when using bare HY under dark and visible light conditions, respectively. The porosity of the catalyst surface may play an important role in adsorption, as previously reported for liquid–gas adsorption systems used to treat wastewater [56]. The use of EGZnO under visible light resulted in 14.5% decolorization of MB, which was 15 times higher than the same reaction under dark conditions. However, the removal percentage increased up to 80.4% when using 1 wt% EGZnO/HY. Proper distribution of the EGZnO nanoparticles on the surface of the HY might facilitate their surface contact with light, which led to higher efficiency of decolorization. This result reveals that EGZnO/HY is a potential photocatalyst semiconductor. Fig. 12b shows the UV spectra of the progress of MB decolorization during the 6 h contact time and the color change before and after the reaction.

3.2.2. Effect of pH

pH is one of the most important parameters that influences the rate of photocatalytic [57]. However, the interpretation of the effect of pH is difficult because of its multiple roles including electrostatic interactions between the catalyst surface, solvent molecules, and substrate, and charged radicals formed during the reaction [12]. Herein the effect of pH was studied in the range of 1–11 in presence of 1 wt% EGZnO/HY catalyst under visible light condition, and the results are presented in Table 3. Each experiment was performed under dark conditions for 2 h to reach an adsorption–desorption equilibrium prior to photocatalytic reaction. The highest decolorization was obtained at pH 3 with a total decolorization of 80.4%, whereas the others were 7.5%, 35.2%, 29.8%, and 19.1%, for pH 1, pH 5, pH 9, and pH 11, respectively. At pH 1, the pH environment was considered to be saturated with the excess of H^+ ions, thus inhibiting the MB from being adsorbed as well as photodecolorized. However, lowering the acidic condition may reduce the amount of positive charges on the surface of the catalyst, thereby resulting in added attraction of MB toward its surface, which facilitates the formation of more hydroxyl radicals from an active catalytic species of EGZnO and thus enhancing the MB decolorization up to 80.4% after 6 h of contact time. In contrast, further increase in pH, decreases the ability of the photocatalytic activity due to saturation

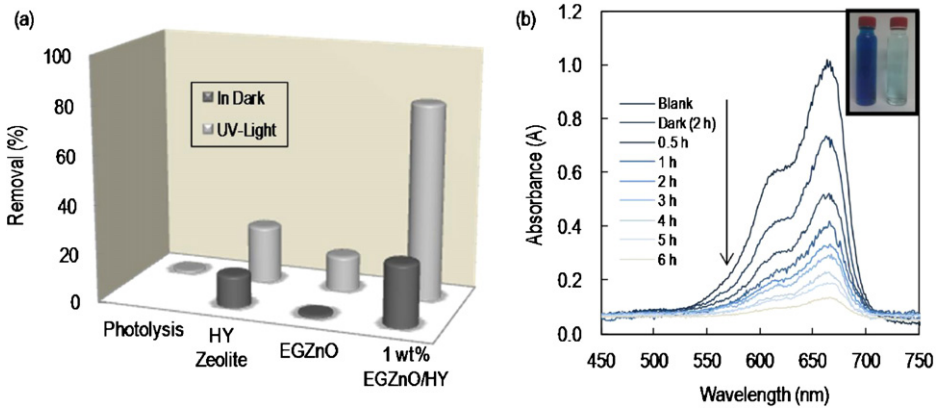

Fig. 12. (a) Photolysis and photocatalysts performance on decolorization of MB (b) color change before and after the reaction and UV spectra of the decolorization progress (C_{MB} = 10 mg L^{-1}, pH 3, W = 0.375 g L^{-1}, t = 6 h, 1 wt% EGZnO/HY).

Table 3
Photodecolorization of MB dye as a function of experiment key factors.

t (h)	Decolorization (%)													
	pH[a]					EGZnO loading[b] (wt%)				EGZnO/HY dosage[c] (g L^{-1})				
	1	3	5	9	11	0.5	1	3	5	0.125	0.250	0.375	0.500	0.625
0.5	0.8	17.6	12.8	5.9	2.7	3.6	17.6	4.1	2.0	1.0	1.8	17.6	5.8	6.3
1.5	2.2	32.3	14.8	11.2	5.4	6.9	32.3	9.3	7.3	4.3	5.3	32.3	17.0	14.9
2.0	3.7	56.3	19.2	15.3	8.3	13.0	56.3	17.4	15.4	4.7	12.2	56.3	28.3	23.1
4.0	4.9	68.1	24.7	22.4	13.7	22.1	68.1	30.2	25.8	8.1	24.0	68.1	44.4	40.3
6.0	7.5	80.4	35.2	29.8	19.1	39.2	80.4	45.8	39.1	12.8	35.0	80.4	55.9	52.5

[a] (C_0 = 10 mg L^{-1}, W = 0.375 g L^{-1}, t = 6 h, 1 wt% EGZnO/HY, 303 K).
[b] (C_0 = 10 mg L^{-1}, pH 3, W = 0.375 g L^{-1}, t = 6 h, 303 K).
[c] (C_0 = 10 mg L^{-1}, pH 3, t = 6 h, 1 wt% EGZnO/HY, 303 K).

as well as highly contamination of the catalyst surface by the MB, thus inhibiting the light penetration, which is most crucial factor for generating an electron–hole pair. The amphoteric behavior also influences the surface charge properties of the catalyst when the photoreaction occurs on the surface of semiconductor [58]. This behavior can be described on the basis of zero point charge (pH_{zpc}) of the EGZnO/HY, which was determined to be at pH 5.2 (Fig. 13). At pHs higher than pH_{pzc}, the surface of the EGZnO/HY became negatively charged and electrostatically adsorbed the positively charged MB cations. Therefore, the photoreaction was not performed well in alkaline conditions. The same phenomenon was observed in the decolorization of methylene blue in presence of TiO_2/ZnS nanocomposites [59].

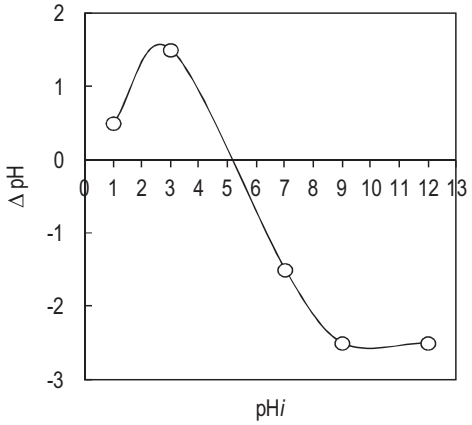

Fig. 13. The isoelectric point (pH_{pzc}) of the EGZnO/HY catalyst.

3.2.3. *Effect of EGZnO loading*

To study the effect of various EGZnO loading, different catalysts were prepared with different amounts of EGZnO loading on HY ranging from 0.5 wt% to 5 wt%. An increase in EGZnO loading resulted in a decrease on the decolorization rate of MB, and 1 wt% of EGZnO was found to be the optimum zinc loading in the range studied, with maximum decolorization of 80.4% was observed after 6 h of contact time (Table 3). The surface area analysis data obtained from the BET method as well as the pore volume and pore diameter determined by the Barret–Joyner–Halenda (BJH) desorption isotherms method can be used to verify this result (Table 4). The increase in EGZnO loading decreases the surface area and pore volume, but increases the pore diameter. The decrease in pore volume was also confirmed by the pore blockage shown in Fig. 14. This may be because of a reflection of the uneven particle sizes of the catalyst. A higher pore volume with a smaller pore diameter appears to enhance the photocatalytic activity [30]. Therefore, the increase in EGZnO loading led to agglomeration on the support surface, resulting in pore blockage and it reduces the surface contact of HY with light as well as the attraction of MB toward the catalysts surface. Increasing the zinc loading increased the formation

Table 4
The textural properties of the catalysts.

Catalysts	Surface area (m^2 g^{-1})	Average pore diameter[a] (nm)	Pore volume (cm^3 g^{-1})
EGZnO	61.3	6.37	0.263
HY	557	2.69	0.376
0.5 wt% EGZnO/HY	549	2.71	0.301
1 wt% EGZnO/HY	420	2.73	0.213
3 wt% EGZnO/HY	403	2.85	0.208
5 wt% EGZnO/HY	347	2.96	0.182

[a] Adsorption average pore diameter (4 V/V by BET).

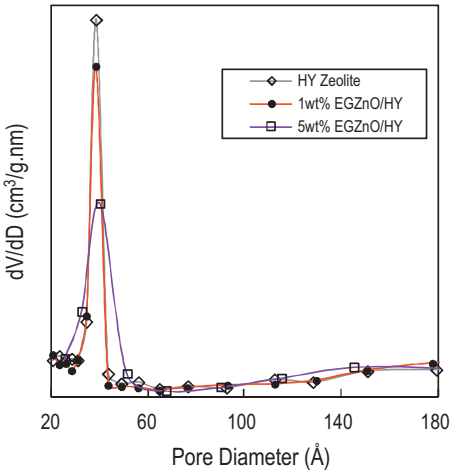

Fig. 14. Pore size distribution curves of the photocatalysts.

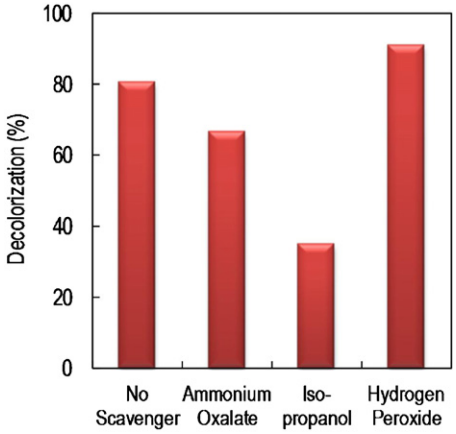

Fig. 15. Effect of different scavengers on photocatalytic decolorization of MB (C_0 = 10 mg L^{-1}, pH 3, W = 0.375 g L^{-1}, t = 6 h, 1 wt% EGZnO/HY).

of Si—O—Zn bonds, which simultaneously decrease the formation of active species of EGZnO. As a result the photodecolorization percentage of MB is lessened. Similar observation was also reported on photoreduction of methyl orange by TiO_2 supported on a zeolite matrix [60,61]. The high crystallinity exhibited by the 1 wt% EGZnO/HY (Fig. 2a) may also explain its higher photocatalytic activity compared to other catalysts tested [12,32].

3.2.4. Effect of catalyst dosage

Table 3 shows the effect of catalyst dosage on MB decolorization ranging from 0.125 to 0.375 g L^{-1}. The increase in decolorization is most likely due to an increase in the number of active sites with higher catalyst loading contributing to an increase in the number of photons and dye molecules absorbed [32]. The most effective decolorization of MB was achieved with a catalyst dosage of 0.375 g L^{-1}, and a further increase in catalyst dosage resulted in a decrease in decolorization. A higher particle concentration leads to a higher turbidity of the suspension, which reduces light penetration and inhibits photodecolorization [62].

3.2.5. Effect of different scavengers

According to Zhang and his co-workers, the hydroxyl radical can be categorized either in form of diffusing or free •OH [63]. The effect of scavenging agents such as ammonium oxalate (AO) as a hole-capturer (H^+) and isopropanol as a diagnostic tool for the radical diffusing (•OH), toward the decolorization of MB was investigated under optimum conditions. As shown in Fig. 15, the presence of these scavengers lowered the rate of photocatalytic activity in the system. The addition of AO enhanced the separation rate between electrons and holes. However, the system was interfered due to the hole-captured by AO and the organic dyes was only mineralized by the free ·OH formed by the reaction of $O_2^{\bullet -}$ when electron was captured by O_2 [64]. Thus, a lower percentage decolorization of MB was obtained, showing that the free •OH is an important species in the photocatalytic process. Besides, isopropanol significantly inhibited the photocatalytic activity; this may be due to the quenching effect [63,65]. On the other hand, the presence of hydrogen peroxide (H_2O_2) in the reaction led to the formation of free •OH and increased the photodecolorization up to 91%. Similar result was also observed for enhanced oxidation of organic pollutants by TiO_2 catalyst in the presence of small amount of H_2O_2 [66]. The enhanced photodegradation efficiency in the presence of H_2O_2 may be due to the free •OH produced either directly via conduction band electrons or indirectly via $O_2^{\bullet -}$ [65].

Indeed, the photocatalytic decolorization of MB in the absence of scavenger, involved the irradiation of EGZnO/HY which generated an electron–hole pair and Zn^{2+} ions [17],

$$\mathrm{EGZnO} + h\nu \rightarrow \mathrm{EGZnO}\left(h_{VB}^{+} + e_{CB}^{-}\right) \quad (5)$$

$$\mathrm{EGZnO}\left(\mathrm{Zn}^{2+}\right) \rightarrow \mathrm{EGZnO}_{\mathrm{vacancy}} + \mathrm{Zn}^{2+} \quad (6)$$

The electron in the conduction band (e_{CB}^-) is highly potential and negatively enough to reduce Zn^{2+} to Zn^+ and then re-oxidize Zn^+ to Zn^{2+} to ensure the formation of $O_2^{\bullet}$ radicals. Subsequent reaction of the Zn^+ with the partial $O_2^{\bullet}$ radicals results in the formation of H_2O_2.

$$\mathrm{EGZnO}\left(\mathrm{Zn}^{2+}\right) + e_{CB}^{-} \rightarrow \mathrm{EGZnO}\left(\mathrm{Zn}^{+}\right) \quad (7)$$

$$\mathrm{EGZnO}\left(\mathrm{Zn}^{+}\right) + \mathrm{O_2} \rightarrow \mathrm{EGZnO}\left(\mathrm{Zn}^{2+}\right) + \mathrm{O_2}^{\bullet} \quad (8)$$

$$\mathrm{H}^{+} + \mathrm{O_2}^{\bullet} \rightarrow \mathrm{HO_2}^{\bullet}\,(\text{partial } \mathrm{O_2}^{\bullet}) \quad (9)$$

$$\mathrm{EGZnO}\left(\mathrm{Zn}^{+}\right) + \mathrm{HO_2}^{\bullet}\,(\text{partial } \mathrm{O_2}^{\bullet}) + \mathrm{H}^{+} \rightarrow \mathrm{EGZnO}\left(\mathrm{Zn}^{2+}\right) + \mathrm{H_2O_2} \quad (10)$$

On the other hand, the valence band hole (h_{VB}^+) is positively enough to generate free •OH and led to direct (Eq. (19)) and indirect (Eqs. (12) and (18)) oxidation of the dye [12].

$$\mathrm{OH}_{\mathrm{ads}}^{-} + h_{VB}^{+} \rightarrow {}^{\bullet}\mathrm{OH}_{\mathrm{ads}} \quad (11)$$

$$\mathrm{H_2O_{ads}} + h_{VB}^{+} \rightarrow {}^{\bullet}\mathrm{OH_{ads}} + \mathrm{H}^{+} \quad (12)$$

The electrons in the conduction band (e_{CB}^-) on the catalyst surface can also reduced O_2 to $O_2^{\bullet -}$ (Eq. (13)).

$$\mathrm{O_{2(ads)}} + e_{CB}^{-} \rightarrow {}^{\bullet}\mathrm{O}_{2\,\mathrm{ads}}^{-} \quad (13)$$

The $O_2^{\bullet -}$ species is responsible for the production of free hydroxyl and hydrogen peroxides radicals:

$${}^{\bullet}\mathrm{O}_{2(\mathrm{ads})}^{-} + \mathrm{H}^{+} \rightarrow \mathrm{HO}_{2(ads)}{}^{\bullet} \quad (\text{in acidic medium}) \quad (14)$$

$$2\mathrm{OH_{ads}}^{\bullet} \rightarrow \mathrm{O_2} + \mathrm{H_2O_2} \quad (15)$$

$$\mathrm{H_2O_2} + {}^{\bullet}\mathrm{O}_{2(\mathrm{ads})}^{-} \rightarrow \mathrm{O_2} + \mathrm{HO}^{\bullet} + \mathrm{HO}^{-} \quad (16)$$

$${}^{\bullet}\mathrm{O}_{2(\mathrm{ads})}^{-} + \mathrm{HO}_{2(\mathrm{ads})}{}^{\bullet} + \mathrm{H}^{+} \rightarrow \mathrm{H_2O_2{+}O_2} \quad (17)$$

Thus, it can be concluded that the Zn^{2+} of the EGZnO are active catalytic species that led to the formation of three highly reactive radicals including the •OH, $HO_2^{\bullet}$ and $O_2^{\bullet -}$ radicals that participated in the MB oxidation. The high oxidation potential of the holes (h_{VB}^+)

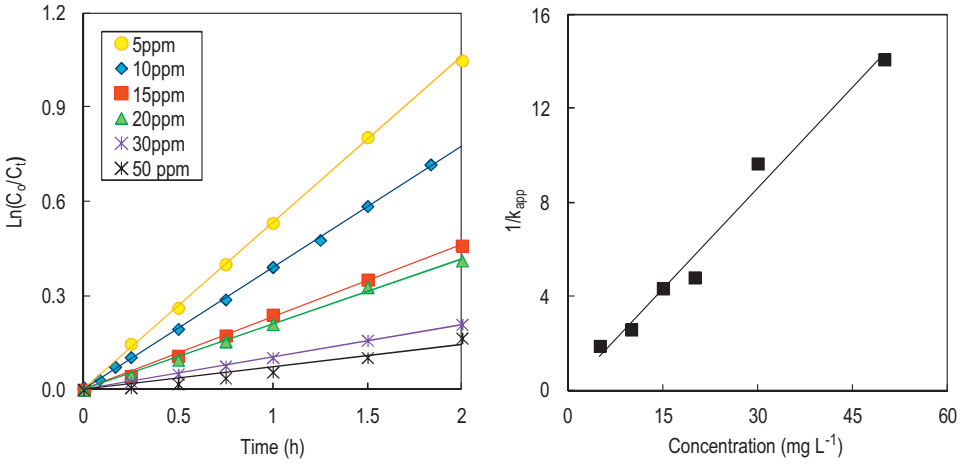

Fig. 16. (a) Photodecolorization kinetics of MB using 1 wt% EGZnO/HY at different MB concentrations and (b) the relationship between $1/k_{app}$ and initial concentration of MB.

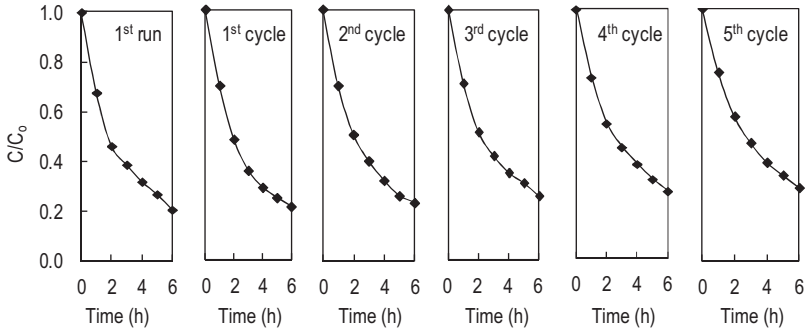

Fig. 17. Reusability of 1 wt% EGZnO/HY on photocatalytic decolorization of MB (C_0 = 10 mg L^{-1}, pH 3, W = 0.375 g L^{-1}, t = 6 h).

in the catalyst also permits the direct oxidation of MB to reactive intermediates.

$$\text{Dye} + \text{OH}^{\bullet} \rightarrow \text{decolorization of dye} \quad (18)$$

$$\text{Dye} + h^{+}_{VB} \rightarrow \text{oxidation of dye} \quad (19)$$

$$\text{Dye} + e^{-}_{CB} \rightarrow \text{reduction of dye} \quad (20)$$

3.3. Kinetic analysis

To study the kinetics of MB photodecolorization, a series of reactions at different initial concentrations of MB ranging from 5 to 50 mg L^{-1} at pH 3 were performed. Generally, the influence of the initial concentration of the solution on the photocatalytic decolorization rate of most organic compounds is described by pseudo first-order kinetics, which is rationalized in terms of the Langmuir–Hinshelwood model modified to accommodate reactions occurring at solid–liquid interface [67]. At low initial dye concentrations, the simplest equation for the rates of photodecolorization of MB is given by [68],

$$\ln C_t = -kt + \ln C_0 \quad (21)$$

where k is the pseudo first-order rate, C_0 and C_t are the concentrations of MB at initial and time t, respectively. The integration of Eq. (21) yields Eq. (22),

$$\ln\left(\frac{C_0}{C_t}\right) = kt \quad (22)$$

The straight line resulting from a plot of $\ln(C_0/C_t)$ as a function of time shown in Fig. 16a confirmed that MB photodecolorization catalyzed by EGZnO/HY follows first-order kinetics. The slope of the line is the apparent first-order rate constant (k_{app}). The values of k obtained from our experiments are listed in Table 5 and reveal a significant and favorable effect of EGZnO/HY on the photodecolorization of MB. A lower concentration of MB results in a higher first-order rate constant, demonstrating the suitability of the system for low dye concentrations. Indeed, the concentrations of dyes in the wastewater from textile industry effluents are always low [69].

Hypothetically, the photodecolorization of MB by EGZnO/HY could be an interface process [68], which might follow the Langmuir–Hinshelwood model (Eqs. (23) and (24)),

$$r_0 = -\frac{dC}{dt} = \frac{K_R K_{LH} C_0}{1 + K_{LH} C_0} = k_{app} C_0 \quad (23)$$

$$\frac{1}{k_{app}} = \frac{1}{K_R K_{LH}} + \frac{C_0}{K_R} \quad (24)$$

where K_R is the reaction rate constant and K_{LH} is the Langmuir–Hinshelwood adsorption equilibrium constant.

A linear plot was obtained by plotting $1/k_{app}$ as a function of C_0 (Fig. 16b) indicating that the photodecolorization of MB by

Table 5
The parameters of photodecolorization at different initial concentration of MB.

Initial concentration (mg L^{-1})	Reaction rate, k (h^{-1})	Initial reaction rate, r_0 (mg L^{-1} h^{-1})	Decolorization (%)
5	0.529	2.65	93.6
10	0.387	3.87	80.4
15	0.231	3.47	60.9
20	0.209	4.18	52.5
30	0.104	3.12	35.2
50	0.071	3.55	22.4

Table 6
Percentage of Zn detected in the solution after experimental determined by ICP-MS.

Catalysts	% Zn detected in the solutions
0.5 wt% EGZnO/HY	No
1 wt% EGZnO/HY	No
3 wt% EGZnO/HY	0.17
5 wt% EGZnO/HY	0.53

EGZnO/HY is consistent with the Langmuir–Hinshelwood model. The reaction rate constant and the adsorption equilibrium constant were calculated to be $K_R = 3.49\ mg\ L^{-1}\ h^{-1}$ and $K_{LH} = 11.0\ L\ mg^{-1}$, respectively. Because of the value of K_{LH} is larger than K_R, these results suggested that the reaction would occurs both in the bulk solution and at the surface of the catalyst [30,70]. In addition, the number of adsorption sites may be not abundant enough to initiate the reaction [30,71].

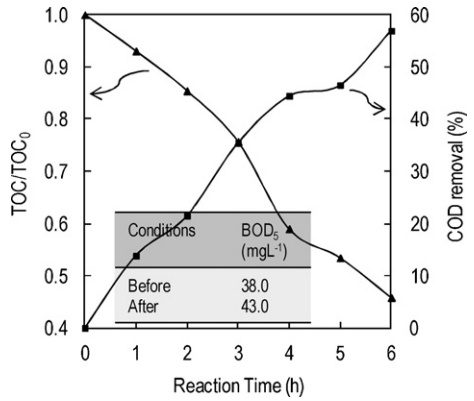

Fig. 18. The graph of COD removal and TOC reduction levels after 6 h of reaction and the insert table are its corresponding BOD_5 ($C_{MB} = 10\ mg\ L^{-1}$, pH 3, $W = 0.375\ g\ L^{-1}$, $t = 6$ h, 1 wt% EGZnO/HY).

3.4. Leaching and reusability of photocatalyst

To study the effect of zinc leaching into the solution, samples of experiment for different weight percent loading of EGZnO loading, irradiated under fluorescent light, were subjected to ICP-MS. The result shows that no Zn ions were detected except for the 3 wt% and 5 wt% EGZnO loading (Table 6) indicating the photocatalytic occurred mainly due to Zn, which exists on the catalyst surface.

A repeat experiment was performed with 1 wt% EGZnO/HY catalyst to study the stability of the catalyst for MB decolorization (Fig. 17). The initial concentration of MB was maintained constant ($10\ mg\ L^{-1}$) at pH 3 and 6 h irradiation time, and the catalyst was

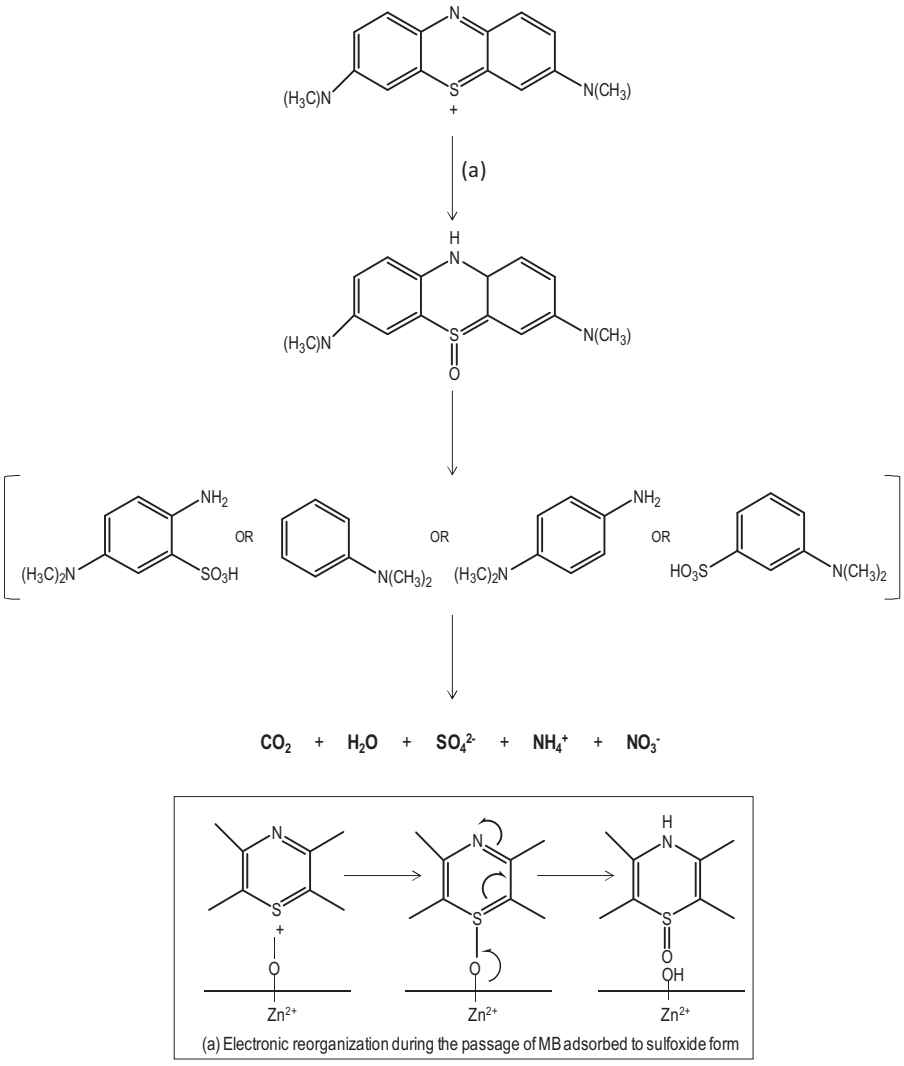

Fig. 19. Suggested photocatalytic degradation pathway of MB [17,64].

recycled after filtration and calcination at 823 K for 3 h at every cycle. It can be observed that after five repeated experiments, the catalyst was still active, with just small decrease in decolorization percentage from 80.4% to 71.1%. The heat treatment most probably induced the catalyst aggregation after several recycles, which resulted in decrease of surface area finally leading to a decrease in photocatalytic efficiency [72].

3.5. Investigation on biodegradability

The chemical oxygen demand (COD), total organic carbon (TOC), and biochemical oxygen demand (BOD) for MB solution were measured and the results are shown in Fig. 18. In the present case, COD indirectly determines the amount of organic compounds present in the aqueous solution. The initial COD values of dye solutions of concentration 10 mg L^{-1} were measured as 144 mg L^{-1}. After irradiation with fluorescent light for 6 h, it only shows 57% of COD removal, which is less than the percent of decolorization of MB (80%). From this result, it can be concluded that the destruction of the chromophoric group of the dye molecules is only responsible for decolorization [73]. The destruction occurs when MB is adsorbed onto the catalyst surface to form sulfoxide compound via electronic reorganization (conjugation). Then, the sulfoxide form was dissociated into most probable benzene ring compounds, resulting in only partial mineralization of the dye molecule [73]. Therefore, herein we proposed the mechanism of the photocatalytic degradation pathway of MB as demonstrated in Fig. 19 [17,74]. The TOC reduction was also measured and it shows only a slight decrease in terms of TOC/TOC_0 ratio, which resulted in 0.46. This type of decrease may attribute to the fact that structured dye molecules were fragmented into small organic molecules during irradiation [73]. These small molecules, which could not be completely removed during the irradiation, contributed considerably to the TOC. In addition, the five days biochemical oxygen demand (BOD_5) was determined to investigate the amount of oxygen, which is consumed by the microorganism to degrade the organic matter during a five days period shown in the insert table in Fig. 18. Note that the BOD_5/COD ratio can be used as a biodegradability index for the aqueous dye solution [75]. Therefore, the BOD_5/COD ratio of the non-irradiated dye solutions was observed 0.26 which indicates that the dye solutions are non-biodegradable. However, after irradiation for 6 h, the ratio increased up to 0.69 suggesting that the non-biodegradable dye solution became biodegradable.

4. Conclusions

In this study, an EGZnO/HY catalyst was prepared by a simple electrochemical method. The physicochemical properties of the prepared catalysts were studied by XRD, TG-SDTA, FE-SEM, TEM, FTIR, UV–vis DRS, PL, surface area analysis, XPS, ^{29}Si and ^{27}Al MAS NMR, and ICP-MS. The results show that nanoparticles EGZnO with less than 30 nm in size were formed and well distributed on the surface of the HY, which showed a high photoactivity toward the decolorization of MB dye. In parallel, an isomorphous substitution of Al with Zn also occurred in the aluminosilicate framework during the electrolysis to give Si—O—Zn bonds, which in contrast, hinder decolorization. An amount of 0.375 g L^{-1} 1 wt% EGZnO/HY was found to be the optimum loading, which resulted in 80% decolorization at pH 3 after 6 h of contact time under visible light irradiation. Based on PL study, it is verified that 1 wt% EGZnO/HY is the most effective photocatalyst. Addition of ammonium oxalate and isopropanol decreased the rate of photocatalytic activity, but presence of H_2O_2 increased in the decolorization of MB. The kinetics studies showed the decolorization followed pseudo first-order kinetics, and the rate constants were determined using the Langmuir–Hinshelwood model, indicating that $K_R = 3.49$ mg L^{-1} h^{-1} and $K_{LH} = 11.0$ L mg^{-1}, respectively, suggesting that the reaction would occur in the bulk solution as well as at the surface of the catalyst. In addition, the number of adsorption sites may be not abundant enough to initiate the reaction. The mineralization of MB was measured by COD removal, BOD_5/COD and TOC/TOC_0 ratio analyses, which achieved 56.9%, 0.69, and 0.46, respectively, after 6 h of contact time. The structure and morphology of the catalyst were still stable after five cycling runs and the leaching test showed negligible leaching effect. In this simple preparation method, a low amount of metal loading was required, and the method exhibited high efficiency toward decolorization of dye. This system exhibits a great potential for improving the quality of the wastewater discharged from textile and other industries.

Acknowledgement

The authors are grateful for the financial support by the Research University Grant from Universiti Teknologi Malaysia (Grant No. 01H59), the awards of UTM Zamalah Scholarship (Norzahir Sapawe) and the Hitachi Scholarship Foundation for their support.

References

[1] B.H. Hameed, E. Khaiary, J. Hazard. Mater. 155 (2008) 601–609.
[2] N. Sapari, Desalin 106 (1996) 179–182.
[3] K. Kadirvelu, M. Kavipriya, C. Karthika, M. Radhika, N. Vennilamani, S. Pattabhi, Bioresour. Technol. 87 (2003) 129–132.
[4] O. Hamdaoui, M. Chiha, Acta Chim. Slov. 54 (2007) 407–418.
[5] C.S.D. Rodrigues, L.M. Madeira, R.A.R. Boaventura, J. Hazard. Mater. 172 (2009) 1551–1559.
[6] A.A. Jalil, S. Triwahyono, S.H. Adam, N.D. Rahim, M.A.A. Aziz, N.H.H. Hairom, N.A.M. Razali, M.A.Z. Abidin, M.K.A. Mohamadiah, J. Hazard. Mater. 181 (2010) 755–762.
[7] F. Harrelkas, A. Azizi, A. Yaacoubi, A. Benhammou, M.N. Pons, Desalin 235 (2009) 330–339.
[8] M. Panizza, G. Cerisola, Appl. Catal. B: Environ. 75 (2007) 95–101.
[9] J.S. Wu, L.H. Liu, K.H. Chu, S.Y. Suen, J. Membr. Sci. 309 (2008) 239–245.
[10] R.A. Damodar, S.J. You, S.H. Ou, Sep. Purif. Technol. 78 (2010) 64–71.
[11] D. Robert, Catal. Today 122 (2007) 20–26.
[12] N. Talebian, M.R. Nilforoushan, Thin Solid Films 518 (2010) 2210–2215.
[13] M. Aleksic, H. Kusic, N. Koprivanac, D. Leszczynska, A.L. Bozic, Desalin 257 (2010) 22–29.
[14] W. Zhang, K. Wang, Y. Yu, H. He, Chem. Eng. J. 163 (2010) 62–67.
[15] W. Zhao, L. Feng, R. Yang, J. Zheng, X. Li, Appl. Catal. B: Environ. 103 (2011) 181–189.
[16] Z.M. El-Bahy, M.M. Mohamed, F.I. Zidan, M.S. Thabet, J. Hazard. Mater. 153 (2008) 364–371.
[17] A. Nezamzadeh-Ejhieh, S. Hushmandrad, Appl. Catal. A: Gen. 388 (2010) 149–159.
[18] R. Prihodko, I. Stolyarova, G. Gunduz, O. Taran, S. Yashnik, V. Parmon, V. Guncharuk, Appl. Catal. B: Environ. 104 (2011) 201–210.
[19] M.J. Height, S.E. Pratsinis, O. Mekasuwandumrong, P. Praserthdam, Appl. Catal. B: Environ. 63 (2006) 305–312.
[20] K. Hayat, M.A. Gondal, M.M. Khaled, S. Ahmed, A.M. Shemsi, Appl. Catal. A: Gen. 393 (2011) 122–129.
[21] J. Liqiang, Q. Yichuan, W. Baiqi, L. Shudan, J. Baojiang, Y. Libin, F. Wei, F. Honggang, S. Jiazhong, Sol. Energy Mater. Sol. Cells 90 (2006) 1773–1787.
[22] C. Hariharan, Appl. Catal. A: Gen. 304 (2006) 55–56.
[23] S. Ameen, M.S. Akhtar, Y.S. Kim, H.S. Shin, Appl. Catal. B: Environ. 103 (2011) 136–142.
[24] B. Gong, Q. Peng, J.S. Na, G.N. Parsons, Appl. Catal. A: Gen. 407 (2011) 211–216.
[25] W. Shen, Z. Li, H. Wang, Y. Liu, Q. Guo, Y. Zhang, J. Hazard. Mater. 152 (2008) 172–175.
[26] Z.R. Ranjban, A. Morsali, Ultrason. Sonochem. 18 (2011) 644–651.
[27] A.A. Jalil, N. Kurono, M. Tokuda, Tetrahedron 58 (2002) 7477–7484.
[28] S. Triwahyono, A.A. Jalil, M. Musthofa, Appl. Catal. A: Gen. 372 (2010) 90–93.
[29] N.F. Jaafar, A.A. Jalil, S. Triwahyono, M.N.M. Muhid, N. Sapawe, M.A.H. Satar, H. Asaari, Chem. Eng. J. 191 (2012) 112–122.
[30] N. Sapawe, A.A. Jalil, S. Triwahyono, S.H. Adam, N.F. Jaafar, M.A.H. Satar, Appl. Catal. B: Environ. 125 (2012) 311–323.
[31] A.A. Jalil, N. Kurono, M. Tokuda, Synlett 12 (2001) 1944–1946.
[32] D.P. Das, N. Baliarsingh, K.M. Parida, J. Mol. Catal. A: Chem. 261 (2007) 254–261.
[33] D.M. Fernandes, R. Silva, A.A.W. Hechenleitner, E. Radovanovic, M.A.C. Melo, E.A.G. Pineda, Mater. Chem. Phys. 115 (2009) 110–115.
[34] J.H. Sun, S.Y. Dong, J.L. Feng, X.J. Yin, X.C. Zhao, J. Mol. Catal. A: Chem. 335 (2011) 145–150.

[35] C.J. Lucio-Ortiz, J.R. De la Rosa, A. Hernandez-Ramirez, E.M. Lopez-Cuellar, G. Beltran-Perez, R.D.C.M. Guardiola, Colloids Surf. A: Physicochem. Eng. Aspects 371 (2010) 81–90.
[36] N. Chandra, D.K. Singh, M. Sharma, R.K. Upadhyay, S.S. Amritphale, S.K. Sanghi, J. Colloid Interface Sci. 342 (2010) 327–332.
[37] C. Wang, H. Shi, Y. Li, Appl. Surf. Sci. 257 (2011) 6873–6877.
[38] S. Kongwudthiti, P. Praserthdam, W. Tanakulrungsank, M. Inoue, J. Mater. Process. Technol. 136 (2003) 186–189.
[39] M. Noorjahan, V.D. Kumari, M. Subrahmanyam, L. Panda, Appl. Catal. B: Environ. 57 (2005) 291–298.
[40] H.D. Lutz, J. Henning, H. Haeuseler, J. Mol. Struct. 156 (1987) 143–145.
[41] S. Krijnen, Titanium Epoxidation Catalysts: Zeolite and Silsesquioxane based Materials, Eindhoven University of Technology, Netherlands, 1998.
[42] J. Klinowski, Prog. Nucl. Magn. Reson. Spectrosc. 16 (1984) 237–309.
[43] J. Klinowski, Colloids Surf. 36 (1989) 133–154.
[44] Z. Luan, C.F. Cheng, H. He, J. Klinowski, J. Phys. Chem. 99 (1995) 10590–10593.
[45] R. Anand, S.G. Hegde, B.S. Rao, C.S. Gopinath, Catal. Lett. 84 (2002) 265–272.
[46] H.T. Cao, Z.L. Pei, J. Gong, C. Sun, R.F. Huang, L.S. Wen, J. Solid State Chem. 177 (2004) 1480–1487.
[47] A. Susarrey-Arce, M.A. Hernandez-Espinosa, F. Rojas-Gonzalez, C. Reed, V. Petranovskii, A. Licea, Part. Part. Syst. Char. 27 (2010) 100–111.
[48] Y. Ohtsu, M. Egami, H. Fujita, K. Yukimura, Surf. Coat. Technol. 196 (2005) 81–84.
[49] J.Z. Kong, A.D. Li, X.Y. Li, H.F. Zhai, W.Q. Zhang, Y.P. Gong, H. Li, D. Wu, J. Solid State Chem. 183 (2010) 1359–1364.
[50] H. Jia, H. Xu, Y. Hu, Y. Tang, L. Zhang, Electrochem. Commun. 9 (2007) 354–360.
[51] L.Y. Zhu, X.Q. Wang, G.H. Zhang, Q. Ren, D. Xu, Appl. Catal. B: Environ. 103 (2011) 428–435.
[52] J. Portier, H.S. Hilal, I. Saadeddin, S.J. Hwang, M.A. Subramanian, G. Campet, Prog. Solid State Chem. 32 (2004) 207–217.
[53] K. Maeda, K. Domen, J. Phys. Chem. C 111 (2007) 7851–7861.
[54] J.G. Yu, H.G. Yu, B. Chen, X.J. Zhao, J.C. Yu, W.K. Ho, J. Phys. Chem. B 48 (2003) 13871–13879.
[55] X.Z. Li, F.B. Li, C.L. Yang, W.K. Ge, Photochem. Photobiol. A 141 (2001) 209–217.
[56] H. Chen, A. Matsumoto, N. Nishimiya, K. Tsutsumi, Colloids Surf. 57 (1999) 295–305.
[57] H. Lachheb, E. Puzenat, A. Houas, M. Ksibi, E. Elaloui, C. Guillard, J.M. Herrmann, Appl. Catal. B: Environ. 39 (2002) 75–90.
[58] M.A. Behnajady, N. Modirshala, R. Hamzavi, J. Hazard. Mater. B133 (2006) 226–232.
[59] A. Franco, M.C. Neves, M.M.L. Mobteiro, J. Hazard. Mater. 161 (2009) 545–550.
[60] R. Chatti, S.S. Rayalu, N. Dubey, N. Labhsetwar, S. Devotta, Sol. Energy Mater. Sol. Cells 91 (2007) 180–190.
[61] J. Yang, J. Zhang, L. Zhu, S. Chen, Y. Zhang, Y. Tang, Y. Zhu, Y. Li, J. Hazard. Mater. B137 (2006) 952–958.
[62] E. Bizani, K. Fytianos, I. Poulios, V. Tsiridis, J. Hazard. Mater. 1367 (2006) 85–94.
[63] L.S. Zhang, K.H. Wong, H.Y. Yip, C. Hu, J.C. Yu, C.Y. Chan, P.K. Wong, Environ. Sci. Technol. 44 (2010) 1392–1398.
[64] S. Meng, D. Li, M. Sun, W. Li, J. Wang, J. Chen, X. Fu, G. Xiao, Catal. Commun. 12 (2011) 972–975.
[65] N. Shimizu, C. Ogino, M.F. Dadjour, T. Murata, Sonochemistry 14 (2007) 184–190.
[66] J. Kiwi, C. Pulgarin, P. Peringer, M. Graztel, New J. Chem. 17 (1993) 487–494.
[67] C.S. Turchi, D.F. Ollis, J. Catal. 122 (1990) 178–192.
[68] L.Y. Yang, S.Y. Dong, J.H. Sun, J.L. Feng, Q.H. Wu, S.P. Sun, J. Hazard. Mater. 179 (2010) 438–443.
[69] J. Grzechulska, A.W. Morawski, Appl. Catal. B: Environ. 36 (2002) 45–51.
[70] J. Cunningham, G. Al-Sayyed, J. Chem. Soc. Faraday Trans. 86 (1990) 3935–3941.
[71] Y. Meng, X. Huang, Y. Wu, X. Wang, Y. Qian, Environ. Pollut. 117 (2002) 307–313.
[72] M. Huang, C. Xu, Z. Wu, Y. Huang, J. Lin, J. Wu, Dyes Pigments 77 (2008) 327–334.
[73] J. Paul, K.P. Rawat, K.S.S. Sarma, S. Sabharwal, Appl. Radiat. Isot. 69 (2011) 982–987.
[74] A. Houas, H. Lachheb, M. Ksibi, E. Elaloui, C. Guillard, J.M. Herrmann, Appl. Catal. B: Environ. 31 (2001) 145–157.
[75] K. Swaminathan, K. Pachhade, S. Sandhya, Desalin 186 (2005) 155–164.